

Prospects for gamma-ray observations of Hercules cluster

V. V. Voitsekhovskiy¹

¹Taras Shevchenko National University of Kyiv, Glushkova ave., 4, 03127, Kyiv, Ukraine
v.v.voitsekhovskiy@gmail.com

Abstract

Galaxy clusters (GCs) are the largest and most massive gravitationally bound objects in the large-scale structure of the Universe. Due to keV temperatures of virialized gas in the intracluster medium (ICM) and presence of cosmic rays (CRs), GCs are effective sources of thermal X-ray radiation and non-thermal leptonic (synchrotron) radio emission. GCs are also store-rooms for hadronic CRs, but non-thermal hadronic gamma-ray emission (mainly, due to pp collisions and subsequent pion decay) from GCs has not been detected yet. In this work we simulate the expected non-thermal hadronic gamma-ray and neutrino emission from dominant part of Hercules cluster - GC A2151 - and estimate a perspective of detection of this emission by existing (Fermi-LAT, LHASSO, IceCube) and planned (CTA, IceCube-Gen2) ground-based and space-based detectors.

Key words: Galaxy clusters, Hercules cluster, A2151, gamma-ray emission, neutrino emission.

INTRODUCTION

Galaxy clusters (GCs) are the largest virialized structures in the Universe at the present cosmological time $t_0 = 13.8$ Gyr (a redshift $z_0 = 0.0$) [29]. A growth of initial density fluctuations due to gravitational instability led to the formation of main elements of large scale structure: sheet-like structures, bordered low density voids, and filaments, connected to the high-density nodes - galaxy clusters and superclusters [26]. The total gravitational masses $M_{cl} \sim 10^{14} - 10^{15} M_\odot$ of GCs include dominant contribution of dark matter (about 80 % of mass) and much smaller contribution of baryonic matter ($\sim 15\%$ of mass in intracluster medium (ICM) gas and $\sim 5\%$ of mass in stars/galaxies) [15], [7], [4]. Virial temperatures of ICM plasma $k_B T \sim GM_{cl} m_p / R_{cl}$ in GCs with typical size $R_{cl} \sim 2 - 3$ Mpc are of the order of $1 - 10$ keV, therefore GCs are luminous sources of thermal X-ray emission, with typical luminosities $L_X \sim 10^{44} - 10^{46} \text{ erg s}^{-1}$.

Formation of gravitationally bound and virialised GCs are long-lasting violent process of main halo collapse and substructures' merger, that is often not completed yet. Most clusters have not yet fully relaxed and accretion and merger processes are still ongoing. Magnetohydrodynamic (MHD) flows in ICM and in active galactic nuclei (AGN), rich in shock waves, efficiently accelerate cosmic rays (CR) and enhance/generate magnetic fields in ICM. Once more, in observed $B_{cl} \sim 1 - 10 \mu\text{G}$ GC magnetic fields the time of diffusive escape of CR from GCs $t_{dif} \sim R_{cl}^2 / D(E)$ is of order or larger than the age of Universe for typical value of diffusion coefficient $D(E) \sim 10^{28} (E/10 \text{ GeV})^{0.5} \text{ cm}^2 \text{ s}^{-1}$. As a result, GCs are effective store-rooms for accelerated CR [7] and, therefore, GCs are expected to be promising sources of non-thermal leptonic (synchrotron) radio emission as well as of hadronic (mainly, due to pp collisions and subsequent neutral pion decay) [20], [25].

Indeed, a non-thermal synchrotron radio emission

in MHz – GHz range from relativistic electrons ($E_e \sim 10$ GeV) in clusters' magnetic fields ($\nu_{syn} \sim 4(B_{cl}/1 \mu\text{G})(E_e/10 \text{ GeV})^2 \text{ GHz}$) is widely presented in observations of GCs [28], but non-thermal gamma-ray emission from GCs has not been detected yet [1], [30].

Both non-thermal radio- and thermal X-ray emission, supplemented by data of *Planck* thermal SZ effect, give a valuable information about dark/baryon matter distribution and physical processes in ICM of GCs [2]. In our work we have carried out a modelling of non-thermal hadronic gamma-ray and neutrino emission from Abell cluster A2151 (a dominant part of Hercules cluster) and estimate prospects for gamma-ray observations of A2151 by existing and planned ((Fermi-LAT, LHASSO, IceCube, CTA, IceCube-Gen2) ground-based and space-based detectors. For calculation we use code MINOT [2] and ΛCDM cosmological model with $H_0 = 70 \text{ km s}^{-1} \text{ Mpc}^{-1}$, $\Omega_M = 0.3$, $\Omega_\Lambda = 0.7$.

HERCULES CLUSTER

The nearby ($z=0.0367$) Hercules supercluster is one of the most massive structures in the Local Universe. It is composed by Abell clusters A2151 (the Hercules cluster), A2147 and A2152 [6]. The most prominent GC A2151 with mass $M_{200} = 4.00 \times 10^{14} M_{\odot}$ and size $R_{200} = 1.45$ Mpc includes three subclusters and is still in the processes of collapsing and mergers [3]. There are 7 AGN-type galaxies in central part of A2151, including NGC 6050 in Arp 272 - a pair of interacting galaxies NGC 6050 and IC 1179.

Considered in this paper GC A2151 contains nearly 360 galaxies, and its optical center have coordinates R.A. = 241.34° and Dec = 17.75° [3]. This cluster demonstrates significant division into several substructures, particularly, bright central bimodal subclump A2151C and two fainters - A2151E and A2151N. Based on Chandra and XMM-Newton observation, A2151C also can be divided into two substructures - bright central A2151C(B) and fainter lateral A2151C(F) [27]. According to state of the art sensitivity of our γ -ray detectors, only A2151C has a chance to be detected, so aim of this paper is to inspect this problem.

Physical conditions and spherically-symmetric dark/baryonic matter distribution in ICM of GC are determined mainly by two global GC parameters - its total mass M_{cl} and size R_{cl} . There are several types of characteristic masses that we have used in modelling. M_{500} denotes the mass that is enclosed inside the radius R_{500} , where a mean density (averaged on volume) exceeds critical density 500 times $\rho/\rho_{crit} = 500$. Corresponding values are related to each other by following relation:

$$M_{500} = \frac{4\pi}{3} 500 \rho_{crit} R_{500}^3 \quad (1)$$

Total mass M_{tot} of GC can be expressed as $M_{tot} = M_{HSE}/(1 - b_{HSE})$, where M_{HSE} is the hydrostatic mass derived from hydrostatical equilibrium and $b_{HSE} \sim 0.2$ is the hydrostatic mass bias [22], [24]. Spatial distribution of gas mass fraction in GC $f_{gas}(r)$ is determined as the ratio of the gas mass $M_{gas}(r)$ and the total mass $M_{tot}(r)$ $f_{gas}(r) = M_{gas}(r)/M_{tot}(r)$.

Gas electron density profile $n_e(r)$ is an important parameter for estimating gamma-ray emission, because it is proportional to total gas density $n_{gas}(r)$, that describes the intensity of proton-proton interactions. There are several theoretical models to describe $n_e(r)$, particularly, analytical beta model [10] that was used in this work:

$$n_e(r) = n_{e,0} \left[1 + \left(\frac{r}{r_c} \right)^2 \right]^{-3\beta_{dens}/2} \quad (2)$$

where $n_{e,0}$ is the normalisation factor, r_c is the core radius of density distribution, β_{dens} is the density index.

Thermal gas pressure is also important, because it allows to normalize the number of CR. Electron thermal pressure $P_e(r)$ is often described by Generalized Navarro Frank White (GNFW) profile [18] as an improved version of the earlier Navarro Frenk White profile (NFW) [19]. Universal pressure profile (UPP) for electrons $\mathbb{P}_e(r)$ depends on four parameters: the normalization factor P_0 , the scale radius $r_p = R_{500}/c_{500}$ (where c_{500} is the concentration parameter for region bounded by R_{500}), and three power indices a_p, b_p, c_p , which denote distribution slope for different spatial regions ($r < r_s$, $r \approx r_s$ and $r > r_s$, respectively):

$$\mathbb{P}_e(r) = P_0 \cdot (r/r_p)^{-c_p} \cdot (1 + (r/r_p)^{a_p})^{(c_p - b_p)/a_p} \quad (3)$$

In order to describe physical processes in particular GC, it is necessary to multiply UPP (3) by several scale factors: $P_e(r) = \mathbb{P}_e(r) \times P_{500} \times F_{500}$, where P_{500} is the characteristic pressure [18], [5], which can be determined by mass and cosmological parameters:

$$P_{500} = 1.65 \times 10^{-3} E(z)^{8/3} \left(\frac{M_{500}}{3 \times 10^{14} h_{70}^{-1} M_{\odot}} \right)^{2/3} h_{70}^2 \quad (4)$$

and the corrective factor F_{500} makes modification by mass due to the self-similarity of GC:

$$F_{500} = \left(\frac{M_{500}}{3 \times 10^{14} h_{70}^{-1} M_{\odot}} \right)^{0.12} \quad (5)$$

Here $H_0 = 100h$ km/s/Mpc, $h_{70} = h/0.70$, and $E(z) = H(z)/H(0)$ or $E^2(z) = \Omega_M(1+z)^3 + \Omega_{\Lambda}$.

For ICM with hydrogen $X=0.725$, helium $Y=0.270$ and heavy elements' mass fraction $Z = 1-X-Y = 0.005$, the mean molecular weights are $\mu_{gas} = 0.60$, $\mu_e = 1.15$, and now we can express the pressure, density and temperature of ICM gas through the pressure and number density of ICM electrons [2]:

$$P_{gas}(r) = (\mu_e/\mu_{gas})P_e(r), \rho_{gas}(r) = (\mu_e/\mu_{gas})m_H n_e(r), k_B T_{gas}(r) = \mu_{gas}m_H(P_{gas}(r)/\rho_{gas}(r)) \quad (6)$$

Magnetic field distribution is following matter distribution [8], [16]. Based on magnetic freezing conditions, spatial distribution of magnetic field can be expressed as proportional to some power η_B of density profile: $B(r) = B_0(n_e(r)/n_{e,0})^{\eta_B}$. Normalisation factor B_0 is set to $5\mu G$, as typical value for GCs, that was measured for Coma cluster based on Faraday rotation data. [8].

Spatially-energetic distribution of CR - nuclei (mainly protons, $i=p$) and electrons ($i = e_1$ for primary ICM electrons, $i = e_2$ for secondary electrons produced in inelastic collisions) in ICM can be divided into the product of energetic and spatial distributions:

$$dN_i(E, r)/dE = A_i f_i(E) \phi_i(r) \quad (7)$$

ICM protons and electrons, accelerating on shock waves inside GCs, acquire a power law distribution by energies. In particular, the classic power law with exponential cut-off energy spectrum was used in this work:

$$f_i(E) = A_i \times \left(\frac{E}{E_{0,i}}\right)^{-\alpha_i} \times \exp\left(-\frac{E}{E_{cut,i}}\right) \quad (8)$$

where α_i is the spectral index, and cut-off occurs at energies $E_{cut,i}$ ($i = p, e1$). Normalization factor A_i is determined by the ratio of CR energy to thermal energy inside sphere with radius $r = R_{500}$. This ratio can be calculated as $X_{cr,i,th} = U_{CR,i}(R_{500})/U_{th}(R_{500})$, where U_{CR} and U_{th} are CR and thermal energy, respectively. Typical values are $X_{cr,p,th} \approx 0.02 - 0.10$, $X_{cr,e,th} \approx 0.0001 - 0.001$. Spatial distribution of CR in ICM is related to gas distribution and is approximated by power law dependence:

$$\phi_i(r) = \left(\frac{n_e(r)}{n_e(0)}\right)^{\eta_{CR,i}} \quad (9)$$

It is also important to note such key parameter as the truncation radius R_{trunc} , which is used to denote physical boundaries of region that contains entire GC volume, outside which density drops to zero. There is discontinuity in thermodynamic parameters at this distance from center of GC. It indicates region of accretion shock radius, where kinetic energy of accretion is converted into thermal energy [13]. Size of this region depends on characteristic radius $R_{trunc} = 3R_{500}$.

GAMMA-RAY AND NEUTRINO EMISSION OF A2151

Characteristics of thermal and non-thermal emission of GCs are determined by spatial distribution of matter (dark and barionic), magnetic fields and CR (leptonic and hadronic components) inside ICM. To recover this distributions we can use observational data about thermal X-ray emission and CMB distortions due to the thermal Sunyaev-Zel'dovich (tSZ) effect. These data allow to recover a spatial distribution of partial pressure of electrons $P_e(r)$ and of total pressure of baryonic gas $P_{tot}(r)$ inside ICM. According to presented above formulae we can build then up the distributions of magnetic fields and CR inside ICM.

Recent work [27] presents new observational results concerning thermal X-ray emission and recovering of thermodynamic parameters of ICM plasma of brightest subclumps A2151CB and A2151CF in GC A2151. Corresponding parameters of ICM in subclumps A2151CB and A2151CF we used for modeling of their gamma-ray and neutrino emission, are presented in Table 1. Based on these data, we calculated normalization factor P_0 for pressure profile from Eq. (3). Its value is denoted by star in Table 1. Other parameters of pressure distribution was taken from Plank Universal Profile 2013 [21]. We need also to take into account the gamma-ray flux absorption by interaction with an extragalactic background light (EBL) [9]. For this purpose we have used Python package `ebtable`¹.

Using described above parameters of galaxy cluster and cosmic rays as input ones, we use open available online² Python language-based software MINOT (modeling the intracluster medium (non-)thermal content

¹<https://github.com/me-manu/ebtable/>

²<https://github.com/remi-adam/minot>

and observable prediction tools). MINOT simulates the intracluster diffuse thermal and nonthermal broad-band (from radio- to gamma-ray) and neutrino emission and as an output calculates the multiwavelength observable spectra, profiles, fluxes, and images for the radio (synchrotron), X-ray (thermal Bremsstrahlung), gamma-ray (inverse Compton and hadronic processes), and neutrino (hadronic processes) messengers [2].

Table 1: Simulation parameters

Global Parameters	A2151CB	A2151CF
z	0.0368	0.0368
M_{500} in [$10^{13}M_{\odot}$]	9.08 ± 5.24	3.01 ± 2.11
R_{500} in [kpc]	$803.38^{+113.18}_{-172.13}$	$566.09^{+89.09}_{-158.26}$
R_{trunc} in [kpc]	2410.15	1698.28
helium mass fraction	0.2735	0.2735
metallicity	0.0153	0.0153
abundance	0.43	0.13
hydrostatic mass bias	0.2	0.2
$X_{cr,p} = U_{cr,p}/U_{th}$ inside R_{500}	0.1	0.1
$X_{cr,e1} = U_{cr,e1}/U_{th}$ inside R_{500}	0.01	0.01
$E_{p,min}$ in [GeV]	1.21	1.21
$E_{p,cut}$ in [TeV]	30	30
$E_{p,max}$ in [TeV]	10^6	10^6
Spectral index α_p (Model)	1.5 (PLEC)	1.5 (PLEC)
$E_{e1,min}$ in [keV]	511	511
$E_{e1,break}$ in [GeV]	-	-
$E_{e1,cut}$ in [TeV]	10^6	10^6
$E_{e1,max}$ in [TeV]	10^6	10^6
Spectral index α_{e1} (Model)	2.3 (PL)	2.3 (PL)
Density CR_p model		
$n_{CR,p}(r) \propto n_e(r)^{\eta_{CR,p}}$	$\eta_{CR,p} = 1.0$	$\eta_{CR,p} = 1.0$
Density CR_{e1} model		
$n_{CR,e}(r) \propto n_e(r)^{\eta_{CR,e}}$	$\eta_{CR,e} = 1.0$	$\eta_{CR,e} = 1.0$
Pressure gas model (GNFW):	$P_0 + PUP$	$P_0 + PUP$
P_0 [keV/cm ³]	0.009*	0.0077*
a_p	1.33	1.33
b_p	4.13	4.13
c_p	0.31	0.31
c_{500}	1.81	1.81
Density gas model (beta)		
n_0 [cm ⁻³]	0.00875	0.0049
r_c [kpc]	19.35	10.43
β_{dens}	0.38	0.28
Magnetic field (Eq.(??))		
B_0 [μG]	5	5
η_B	2/3	2/3

Main results of gamma-ray and neutrino emission for A2151CB and A2151CF subclumps are presented in Fig 1-5. The most promising for CTA-detection cases correspond to hard CR spectrum (spectral index $\alpha_p < 2$). In particular, Fig. 1 demonstrates expected gamma-ray flux from the central brightest subclump A2151CB for $\alpha_p = 1.5$ and for three values of cluster mass - average mass and $\pm \Delta m$ from Table 1. Meantime, there is no significant increase in flow due to more compact CR distribution (a result of magnification of $\eta_{CR,p}$ twice is shown in Fig. 2).

For comparing different models of CR distribution in ICM, we have simulated gamma-ray flux for three values of spectral index - see Fig. 3 and Fig. 4. As we can see from these figures, there is a possibility

for CTA to detect the brightest subclump A2151CB in case of hard CR spectrum, instead of A2151CF, that has relatively low flux for all CR distribution models (Fig. 4. Calculated neutrino flux from the brightest subclump A2151CB together with IceCube discovery potential at significance level 5σ is shown in Fig. 5. As we can see from this figure, neutrinos do not suffer from energy losses as photons do due to EBL absorption. This fact can make neutrino emission to be a good probe for GC in the future.

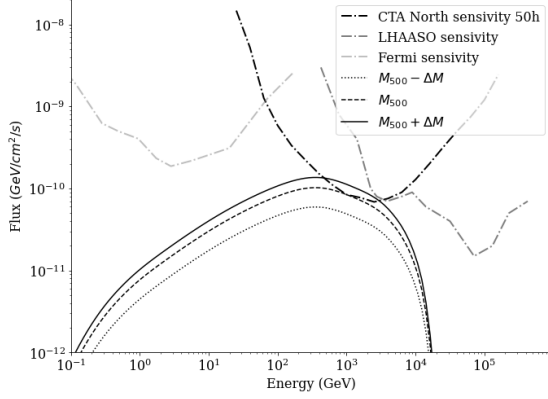


Figure 1: Spectral flux from A2151CB for three values of cluster mass M_{500} and $M_{500} \pm \Delta m$. Other parameters as in Table 1

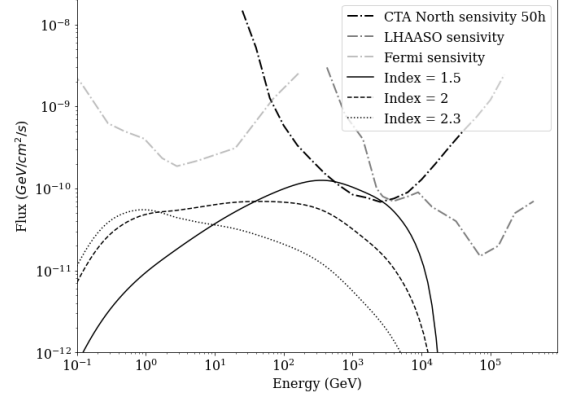


Figure 2: Spectral flux from A2151CB for three values of spectral index. CRs distribution $CRp \propto n_e(r)^2$. Other parameters as in Table 1

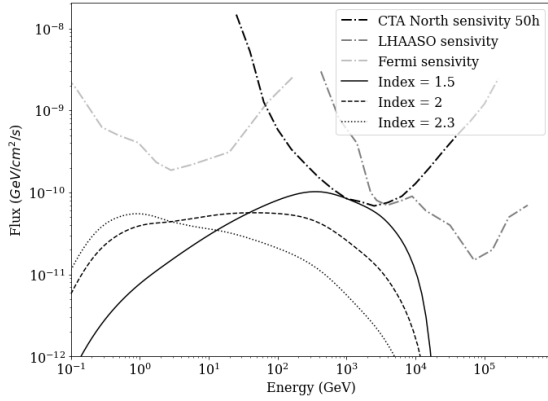


Figure 3: Spectral flux from A2151CB for three values of spectral index. Other parameters as in Table 1

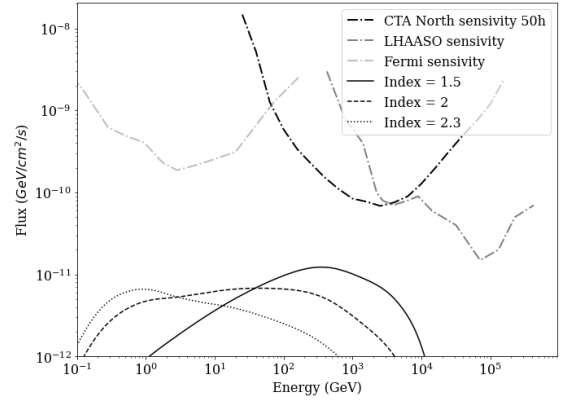


Figure 4: Spectral flux from A2151CF for three values of spectral index. Other parameters as in Table 1

CONCLUSIONS

Due to a long time for cosmic rays diffusion escape, GCs should be a luminous extragalactic sources of neutrino and non-thermal gamma-rays, but such emission has not been detected yet. Using the recent data from [27] about thermal X-ray emission of brightest subclumps A2151CB and A2151CF in GC A2151 we have carried out a modelling of non-thermal hadronic gamma-ray and neutrino emission of these subclumps using MINOT code [2]. Results of our simulations show that under the typical parameters of cosmic ray distribution (cosmic ray proton to thermal energy ratio $X_{cr,p} \approx 0.04 - 0.06$, spectral index of proton power-law energy spectrum $\gamma = 2.5$) both non-thermal hadronic gamma-ray and neutrino emission of subclumps A2151CB and A2151CF are still undetected by existing and planned detectors. Meantime, backreaction of 7 AGN-type galaxies in subclumps A2151CB and A2151CF and other unaccounted for sources of cosmic rays (merging and accretion flows, turbulence etc.) can increase $X_{cr,p} \approx 0.1$ and provide harder spectral index $\gamma = 1.5 - 2.0$. In these cases brighter subclump A2151CB can be detected by CTA at 5σ level. Hard cosmic ray proton spectrum is promising also for detection of neutrino fluxes from GCs in future neutrino detectors (IceCube-Gen2 etc.). Contrary to gamma-ray fluxes, neutrino fluxes do not attenuate by interaction with the

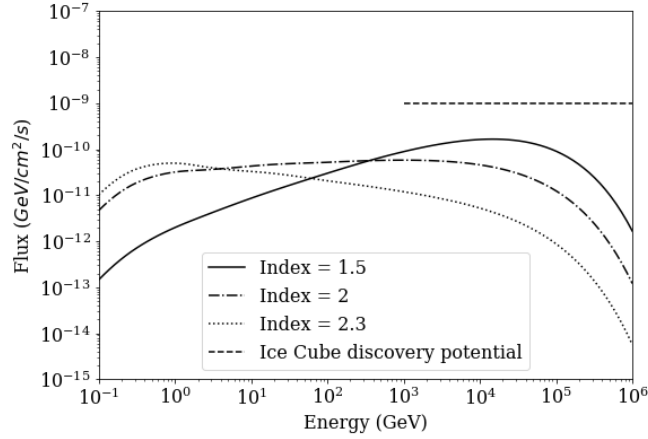


Figure 5: Neutrino flux from the brightest subclump A2151CB with IceCube 5σ discovery potential at 1-1000 TeV [14]

extragalactic background light (EBL), therefore, there are promising possibilities to detect PeV- neutrinos in case of GCs - cosmic PeVatrons with hard ($\gamma < 2.0$) spectra.

References

- [1] Ackermann M., Ajello A., Allafort A. et al., 2014, ApJ, 787, 18
- [2] Adam R., Goksu H., Leingartner-Goth A. et al., 2020, A&A, 644, A70
- [3] Agulli I., Aguerri A. L., Diaferio A., Dominguez Palmero L., Sanchez-Janssen R., 2017, MNRAS, 467, 4410
- [4] Allen S., Evrard A., Mantz A., 2011, ARA&A, 49, 409
- [5] Arnaud M., Pratt G. W., Piffaretti R. et al., 2010, A&A, 517, A92
- [6] Barnby P., Huchra J., 1998, ApJ, 115, 1, 6-25
- [7] Berezhinsky V., Blasi P., Ptuskin V., 1997, ApJ, 487, 529
- [8] Bonafede A., Feretti L., Murgia M. et al., 2010, A&A, 513, A30
- [9] Dwek E., Krennrich F., 2013, Astroparticle Physics, 43, 112
- [10] Cavaliere A., Fusco-Femiani R., 1978, A&A, 70
- [11] Einasto M., Einasto J., Tago E., Müller V., Andernach H., 2001, ApJ, 122, 5
- [12] Gong Y., Ma Y. Z., Tanimura H., 2019, MNRAS, 486, 4
- [13] Hurier, G., Adam, R., Keshet, U., 2019, A&A, 622, A136
- [14] Ice Cube Collaboration et al., The European Physical Journal C, 2019, 79, 234
- [15] Mohr J., Mathiesen B., Evrard A., 1999, ApJ, 517, 627-649
- [16] Murgia M., Govoni F., Feretti L. et al., 2004, A&A 424, 2
- [17] Ma Y. Z., Gong Y. et al, 2021, MNRAS, 500, 2
- [18] Nagai D., Kravtsov A. V., Vikhlinin A., 2007, ApJ, 668, 1
- [19] Navarro J., Frenk C., White S., 1996, ApJ 462, 563
- [20] Pfrommer C., EnBlin T., 2004, A&A, 413, 17-36
- [21] Planck Collaboration et al., 2012, A&A, 550, A131
- [22] Planck Collaboration et al., 2014, A&A, 571, A20
- [23] Planck Collaboration et al., 2016, A&A, 594, A13
- [24] Piffaretti R., Valdarnini R., 2008, A&A, 491, 1
- [25] Pinzke A., Pfrommer C., 2010, MNRAS, 277, 33
- [26] Springel V., Frenk C., White S., 2006, Nature, 440, 1137-1144
- [27] Tiwari J, Pal Singh K., [arXiv:2011.08850v1]
- [28] van Weeren R.J., de Gasperin F., Akamatsu H., Brüggén M., et al., 2019, Space Sci. Rev., 215, 16
- [29] Voit G. M., 2005, Reviews of Modern Physics, 77, 207
- [30] Wittor D., 2021, New Astronomy, 85, 101550